Ionization of Rydberg atoms of sodium by 360–4400 eV alkali-metal ions

Oleg Makarov and K. B. MacAdam
Department of Physics and Astronomy, University of Kentucky, Lexington, Kentucky
(Received 16 March 1999)

Impact ionization by singly charged ions from Rydberg Na($24d$) and Na($25s$) states has been investigated over the reduced velocity region $\tilde{v}=0.5$–2.2. The ions of Na^+, K^+, and Li^+ were accelerated to energies from 360 to 4400 eV and used to bombard the laser-excited Rydberg atoms. Electrons released in the ionization of Rydberg atoms were collected from the collision volume and registered by a channel electron multiplier. Measured relative ionization cross sections from Na($24d$) and Na($25s$) states show maxima at $\tilde{v}=1.6$–1.7 and agree moderately well with classical-trajectory Monte Carlo calculations. [S1050-2947(99)03709-9]

PACS number(s): 34.50.Fa, 34.60.+z

I. INTRODUCTION

Collisional processes are important in many areas of physics research. The broad range of topics includes the study of interaction of matter with radiation in medical processes (e.g., radiation damage in biological matter) and laboratory and astrophysical plasma research (e.g., energy loss of heavy ions in solid targets and plasmas). The ionization of atoms by heavy-ion impact is also of interest in relation to the use of neutral beams to heat plasmas in fusion reactors. The differential and total cross sections for these reactions, even in relative units, are important in many applications.

The experiments reported in this paper study ionization processes of the type

$$X^+ + \mathrm{Na}(n\ell) \rightarrow X^+ + \mathrm{Na}^+ + e^-, \tag{1}$$

where X^+ is a singly charged ion of an alkali-metal element Li^+, Na^+, or K^+ (natural isotope abundances), and Na($n\ell$) is the sodium atom in a Rydberg state having principal quantum number n and angular momentum ℓ. The projectile ion X^+ bombards the atom A, which is a bound system consisting of the singly charged core A^+ and the orbiting electron e^-. The projectile ion X^+ has a velocity v_{ion}. The electron's motion is characterized by root-mean-square velocity $v_{\mathrm{Bohr}}=1/n$ in a.u. After the collision, the atom is ionized, and the electron is ejected, leaving the positive core A^+ behind. In this paper the energy of the projectile ion is expressed in terms of reduced velocity, defined as the ratio of the ion velocity to the Bohr velocity of the electron in the Rydberg state, $\tilde{v}=v_{\mathrm{ion}}/v_{\mathrm{Bohr}}$.

The theory of impact ionization has been studied in various models and approximations. The first Born approximation (FBA) was used by Bates and Griffing to calculate cross sections for the excitation and ionization of a hydrogen atom by proton and hydrogen impact [1]. Subsequent experimental work with ionization of ground-state hydrogen by proton impact [2] showed that the FBA was valid at high impact velocities of the proton (high impact energy region). A treatment of the ionization of a hydrogen atom that improves the simple first-order weak perturbation theory is the continuum-distorted-wave eikonal-initial state (CDW-EIS) introduced by Crothers and McCann [3]. The CDW-EIS model has been widely used by others to obtain improved results [4–7] at moderately high energies. The problem of ionization of atomic hydrogen by slow protons was considered recently by Sahoo *et al.* [8]. They calculated the ionization cross section in heavy-particle collisions in the impact parameter formalism, considering the influence of coupling with the important bound states in direct as well as in rearrangement channels in a two-centered atomic-state expansion. The relevant time-dependent Schrödinger equation was solved by a variational method in the two-state approximation. Their calculation agrees with the data of Refs. [2,9] up to the energy 100 keV.

The two-center atomic orbital (TCAO) close-coupling method has been successfully used in ion-atom collisions in the intermediate impact energy region [10,11], where the reduced velocity of the projectile is of the order of unity, and excitation, capture, and ionization processes are of comparable importance. A triple-center atomic-state method for treating ionization in low-energy ion-atom collision was proposed by Winter and Lin [12,13]. This method intrinsically accounts for the Wannier [14] mechanism, in which the electron will not have been removed in a slow collision unless it is asymptotically at the point of unstable equilibrium between the nuclei, i.e., at the saddle point.

Among the theories that use the laws of classical mechanics in calculating the ionization cross sections are the sudden-impulse or binary encounter (BE) approximation, reviewed by Bates and Kingston [15], and the classical-trajectory Monte Carlo (CTMC) approximation. Classical-trajectory methods are among the best for modeling ion–Rydberg-atom collisions at intermediate velocities. CTMC calculations of the total cross sections for ionization and charge transfer of hydrogen atoms in a fully populated n shell by protons were reported by Abrines and Percival [16,17]. Olson [18] performed classical-trajectory Monte Carlo calculations for collisions of ions in charge states $q=+1,\ +2,\ +5$, and $+10$ with a hydrogenic target atom in shells $n=1,\ 2,\ 5,\ 10$, and 20. In [19], Becker and MacKellar used the CTMC method for ion-atom collisions in the velocity matching region for target Rydberg states of a given specific n and ℓ.

Processes involving sodium atoms as targets were studied by Jain and Winter [20], who employed a two-center coupled-Sturmian-pseudostate approach to calculate the total

and partial electron transfer, target excitation, and ionization cross sections. They studied electron transfer, target excitation, and ionization in collisions of protons at energies 1–100 keV and sodium atoms in $3s$ and $3p$ states.

One of the experimental methods of studying ionization is to measure the yield of electrons. Such measurements of ionization from alkali metals were carried out by O'Hare *et al.* [21], who studied the ionization of potassium and sodium vapor by 20–100 keV H^+ and He^+ ions using a modulated crossed-beam technique. The absolute cross sections σ_e for electron production were determined from the gross yield of electrons. The ionization data were compared with calculations based on both the FBA [22] and the classical sudden-impulse approximation [15] and with experimental data on the ionization of potassium and sodium by electron impact [23]. An experimental study of the ionization of atomic hydrogen by fast H^+ and He^{2+} ions was performed by Shah and co-workers [2,9]. The same group also reported work with slow He^{2+} ions [24] and, most recently, with slow protons [25]. In [2] they measured the cross sections for the ionization of ground-state hydrogen atoms by 38–1500 keV protons and 125–2200 keV α particles. In [9] and [25] they extended the measurements of the ionization of atomic hydrogen atoms by protons down to 9.4 keV and 1.25 keV, respectively, and reported cross section measurements in the energy range from 1.25 keV to 75 keV.

Low-energy electron emission in proton-helium collisions was studied by Bernardi *et al.* [26,27]. They measured electron spectra for ionization of a He target by H^+ projectiles with impact energies of 100 and 200 keV. Electrons having energy from 1 to 16 eV were examined in Ref. [27] and from a few eV to approximately 250 eV in Ref. [26]. In this region of electron energies, the main contribution to the ionization process originates from ''soft'' (or glancing) collisions. They observed a forward-backward asymmetry in the doubly differential cross section and a minimum at the electron ejection angle $\theta = 120°$. Rudd and Madison [28] compared experimental and theoretical doubly differential electron ejection cross sections in helium by proton impact from 5 to 100 keV. They studied this energy range of protons in order to determine the limit of applicability of the FBA to this process. It was shown before [29] that experimental angular distributions of electrons ejected from helium by 100- to 300-keV protons agreed reasonably well with calculations using the scaled hydrogenic FBA at intermediate angles. By replacing the scaled hydrogenic wave functions with more realistic ones, the authors in Ref. [28] obtained good agreement at small and large angles. They found that by using wave functions obtained from a Hartree-Fock potential good agreement between experimental data and theoretical Born calculations could be found at proton energies as low as 5 keV.

While the experiments reviewed above were performed with ground-state targets, ionization measurements have been carried out with laser-excited atoms as well. Electron-impact ionization of laser-excited sodium atoms was reported by Tan *et al.* [30]. They measured the total electron-impact ionization cross sections of laser-excited $3p_{3/2}$ sodium in the energy range from threshold to 30 eV. These cross sections were measured simultaneously for both ground-state and $3p_{3/2}$ excited-state atoms as a function of electron-impact energy. Excited-state data were calibrated with respect to the ground-state data, which were normalized in turn to the previous absolute measurements. The absolute cross section for removal of Rydberg electrons from Na Rydberg atoms by impact of singly charged ions was measured by MacAdam *et al.* [31]. Electron loss, the sum of ionization and charge transfer, was detected by collecting impact-produced Na^+ from the target after a few microseconds exposure to the projectile beam.

In that work, an important correction for excitation and a small correction due to second-order effects had to be applied to all the results, because the authors used a 70-V/cm pulse to sweep impact-produced ions into the detector, which also field-ionized neutral Na that had been excited by impact to sufficiently high states without ionization. In the present work, the electrons released during ionization were swept into the detector by a constant small field, which was approximately 0.6–1.0 V/cm at the location of Rydberg atoms. Whereas a 70-V/cm field would field ionize Rydberg states from $n = 46$ upward, a 1 V/cm field would field ionize only those Rydberg states with $n > 134$. The cross section for excitation into bound states with $n > 134$ is negligible as compared with the total ionization cross section, so none of the corrections made in previous work were necessary. At these small values of electric field, Rydberg atoms with $n \approx 25$ may be considered as being in a field-free region, and the target states were those characterized by quantum numbers n and ℓ.

The work described in this paper focuses on the ionization of highly excited Rydberg atoms by singly charged heavy ions in the energy range corresponding to reduced velocities near one, i.e., in the velocity range near the matching velocity. The maximum in the ionization cross section was observed to occur at a projectile energy slightly above the matching velocity, which is known to be the case also for ground-state ionization. Thus the projectile energy at which ionization is maximum scales approximately as $1/n^2$ along with the binding energy.

II. EXPERIMENTAL SETUP

The ionization measurements were performed by using orthogonally crossed projectile and target beams. A thermal beam of sodium atoms exited from a small aperture in the 200 °C tubular Na oven into a vacuum maintained at 10^{-7} torr. The beam entered an interaction region, defined as the region between two selective field ionization (SFI) condenser plates, through a collimating aperture. The experimental setup is shown in Fig.1. Rydberg atoms were produced from ground-state sodium atoms in a two-step photoexcitation near the point of intersection of atom and ion beams.

Two pulsed laser beams were used to excite sodium atoms to Rydberg states. An unfocused yellow (589.6 nm) laser beam entered the interaction region at an angle of 30° with respect to the atomic beam. A focused blue (410 nm) laser beam entered in the direction opposite to the atomic beam. The intersection of the two laser beams defined a volume in which the Rydberg atoms were excited during each firing of the laser. The blue laser excited the $24d_{3/2}$ fine-structure level.

The planes of polarization of both beams were perpendicular to the direction of the ion beam. The m_ℓ-sublevel

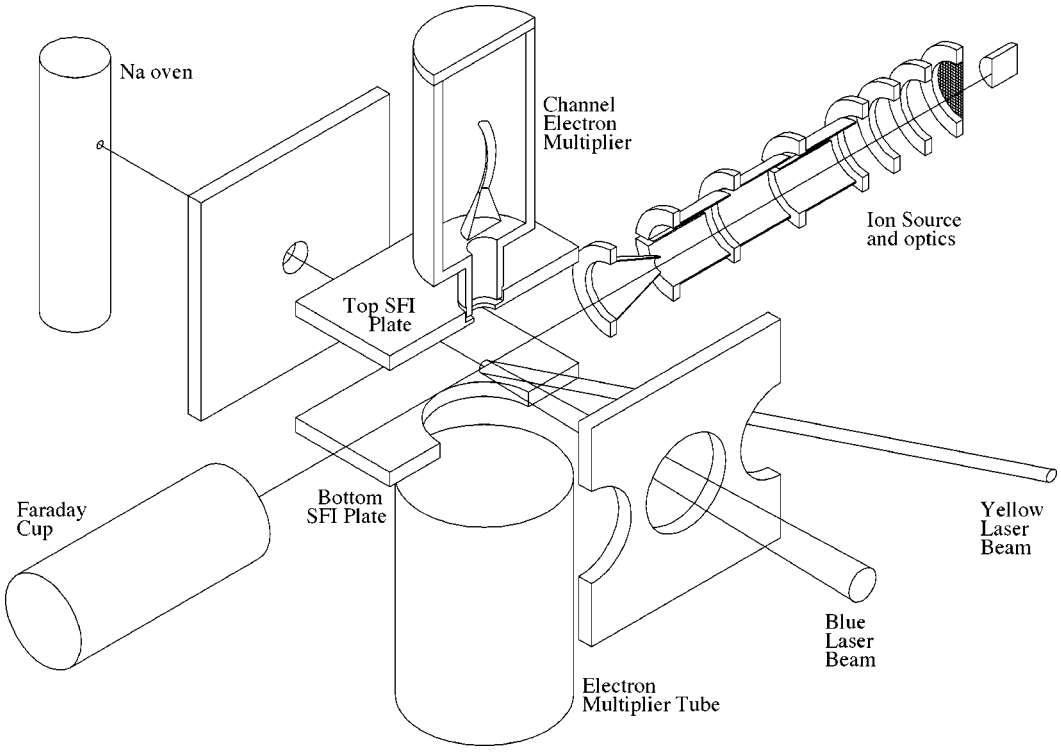

FIG. 1. Experimental setup.

population (with reference to the ion-beam direction) of the nd state may be calculated from Clebsch-Gordan coefficients [32]. For the case of the $3p_{1/2}$ intermediate state, the population of the different m_ℓ sublevels does not depend on the angle of polarization of the yellow beam. For the blue beam with polarization perpendicular to the ion-beam direction, the relative populations of different m_ℓ sublevels of the 24d state are 0.1 for $m_\ell=0$, 0.3 for $|m_\ell|=1$, and 0.6 for $|m_\ell|=2$. Thus, atoms in the 24d state are mostly in a state with the sublevel $m_\ell=\pm 2$. For the 25s target state, the entire population has $m_\ell=0$.

Ions emerged from the ion source, passed through the interaction region, and were measured by a Faraday cup located farther downstream. Ionization occurred as the beam of Rydberg atoms intersected the beam of ions. The Li^+, Na^+, and K^+ ions were produced from thermionic sources [33] and accelerated to suitable energies in an ion gun, which contained ion optics for focusing, steering, and deflection. This produced a collimated ion beam with a diameter 3 mm that entered the interaction region perpendicular to the direction of the atomic beam. The ions were accelerated so that their reduced velocities $\tilde{v}$ lay in the range from 0.5 to 2.2, where

$$\tilde{v}=\frac{v_{\rm ion}}{v_{\rm Bohr}}=0.006\,35n^*\sqrt{\frac{E(\rm eV)}{M(\rm amu)}}. \qquad (2)$$

Here, $n^*=n-\delta_\ell$ is the effective principal quantum munber, δ_ℓ is the quantum defect for the state with orbital angular momentum ℓ, E is the energy of the ion, and M is the ion mass. K^+ ions were used to cover the lowest range of reduced velocities, from $\tilde{v}=0.5$ to $\tilde{v}=1.0$, at corresponding energies from 400 eV to 1700 eV. Na^+ ions were used for the middle range of reduced velocities, from $\tilde{v}=0.7$ to $\tilde{v}=1.2$, at energies from 500 to 1500 eV. To produce an ion beam with the highest achievable reduced velocities, Li^+ ions were accelerated to 350 eV to 1500 eV, which corresponded to reduced velocities from 1.1 to 2.2. Li^+ ions were used only in the case of Na(25s) target atoms. For target atoms in the 24d state, ions of sodium were used instead to cover the upper range of reduced velocities—in which case they were accelerated to energies up to 4400 eV.

The deflection element of the ion optics was formed from two half cylinders. A high deflection voltage was applied to one of them when the ion beam was to be deflected. An exit aperture in the form of a conical shield was placed at the end of the ion optics assembly with a tip of the cone facing toward the ion beam. Placing such an aperture reduced the escape probability of any secondary electrons caused by the ions striking the edge of the aperture. It was also isolated from ground, and an arbitrary positive potential of the order of a few tens of volts could be applied to the aperture that further reduced the background due to secondary electrons. The ion current passing though the interaction region was in the range of a few tens of nA.

The free electrons resulting from collisions between Rydberg atoms and ions were detected individually by a channel electron multiplier (CEM). The CEM also collected background electrons that were unrelated to the collisions under study. One source of background was ionization of Rydberg atoms induced by ambient blackbody radiation. This background occurred only when Rydberg atoms were present and varied linearly with their number. Other sources of background included secondary electrons from ion impact on the metal walls of the apparatus and impact ionization of ambient gas in the interaction region. Backgrounds of these

types were linear in ion current and occurred regardless of the presence of the exciting laser beams. To minimize backgrounds the CEM was totally enclosed in a cylindrical case. The only aperture in the case through which electrons could enter the channel electron multiplier was one that faced the interaction region.

A Galileo Electro-Optics 4039 Channeltron [34] was used in pulse-counting mode. Electrons that were released during the ionization of Rydberg states had small energy, of the order of tens of meV to 1 eV. They were swept into the cylinder by a constant small electric field that penetrated into the interaction region. The top SFI plate had a 6-mm-diameter opening, which was used to allow field penetration and collection of electrons. Calculations performed with SIMION [35] showed that the field resulting from the potential difference applied between the cylinder and the plates was approximately 0.6–1.0 V/cm in the middle of the interaction region, at the location of Rydberg atoms. In order to detect the free electrons more efficiently, they were further accelerated inside the CEM enclosure to energies at which the CEM has a maximum detection efficiency. This was achieved by biasing the front end of the CEM at a few hundred volts with respect to ground.

The CEM pulses were amplified and discriminated, yielding a pulse-pair resolution time 120 nsec. A height discriminator level 100–150 mV blocked most noise pulses without sacrificing the overall counting rate. Discriminator pulses (from both ionization and background) were counted by a gated counter during a 5-μsec interval beginning 5 μsec after each laser shot, and counts were summed by the counter during 256 successive laser shots.

Following a small time delay after the laser flash, and after allowing for collection and registration of ionization signals, a high-voltage pulse was applied to the top SFI plate. The resulting electric field between the SFI plates ionized the remaining Rydberg atoms, and their positive cores were swept into a discrete-dynode electron multiplier tube (EMT) through a meshed opening in the bottom SFI plate. The first dynode (dynode located nearest the bottom SFI plate) was kept at ground potential. This was necessary to minimize CEM background pulses resulting from stray electrons produced outside the electron multiplier, which would otherwise be accelerated across the interaction region by a strong electric field penetrating from the first dynode.

The integrated signal corresponding to the total number of ions in the resulting SFI pulse was used to normalize the number of ionization events to the population of Rydberg states. While the high-voltage pulse was applied to the SFI plates, the ion beam was deflected away from the target in order to avoid contamination of the SFI signal by positive ions from the ion beam. Both SFI plates were biased such that the net field between them was canceled except during the high-voltage pulse. The negative potential of the plates was set at 5–10 V, sufficient to repel stray electrons entering the interaction region from the sides.

III. EXPERIMENTAL METHOD AND RESULTS

The time relationship of signals and gates used for data acquisition is shown in Fig. 2. All time delays were referenced to SYNC OUT of the laser system, which defined the

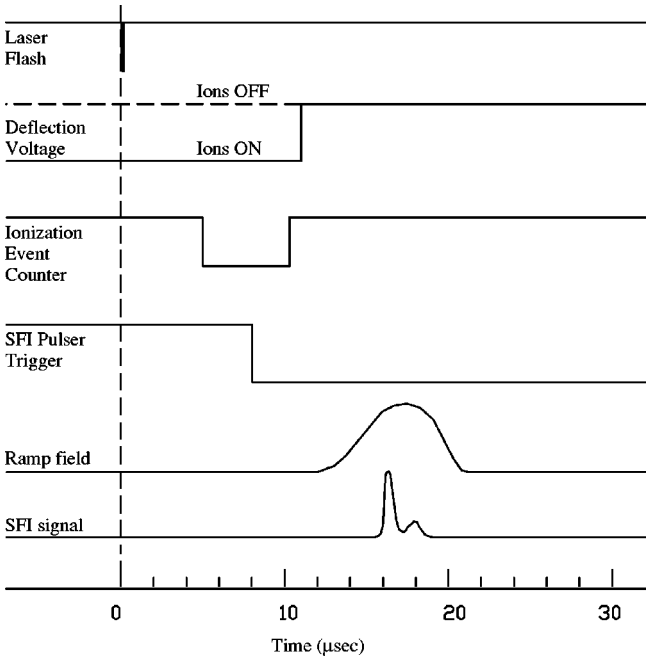

FIG. 2. Timing diagram.

time $t=0$ sec. The average atomic beam velocity was 0.8 mm/μsec. The intersection of the laser beams defined the space where Rydberg atoms were excited. This cloud, consisting of a mixture of ground-state and Rydberg-state Na atoms, was offset by 4–5 mm from the ion-beam axis and was approximately 4 mm long. The Rydberg atoms traveled 4 to 6 μsec before they intersected the ion beam. The impact ionization took place as this cloud of Rydberg atoms crossed the ion beam for another 4–5 μsec, during which the electron pulses were counted. After the Rydberg atoms had crossed the ion beam, the projectile ions were deflected, and the high-voltage pulse was applied to ionize the remaining neutral Rydberg atoms.

The duration of the gate window was set to 5 μsec in order to ensure the collection of all electrons released in ionization events. In order to avoid noise pulses which occurred as the beam-gating voltage was switched on during ions ON, the duration of the counting gate window was shortened accordingly.

For each ion source and for each reduced velocity from the corresponding range the measurement sequence consisted of the following. First, the background pulses were measured during five cycles of 256 laser shots each with the laser being blocked and ions being deflected away, which resulted in an average N_B pulses per cycle. Second, the pulses were counted during three cycles of 256 laser shots each under three different conditions:

(1) The number of pulses N_{L+I} counted with both lasers and ions ON.

(2) The number of pulses N_L counted with lasers ON and ions OFF.

(3) The number of pulses N_I counted with lasers OFF and ions ON.

Also, the integrated SFI pulse area A and the ion current I were measured, which resulted in A_{L+I}, A_L and I_{L+I}, I_I.

TABLE I. Relative ionization cross sections for Na(24*d*) states. SD, standard deviation.

Reduced velocity $\tilde{v}$	σ^{ion} For K^+	SD	σ^{ion} For Na^+	SD	σ^{ion} For all ions	SD
0.5	0.43	0.65			0.43	0.65
0.6	1.30	0.55			1.30	0.55
0.7	1.66	0.52	2.47	1.03	1.82	0.46
0.8	3.37	0.53	3.71	0.67	3.50	0.41
0.9	3.77	0.48	3.95	0.64	3.84	0.38
1.0	4.63	0.50	4.22	0.47	4.41	0.34
1.1			4.36	0.34	4.36	0.34
1.2			6.36	0.37	6.36	0.37
1.3			15.34	0.87	15.34	0.87
1.4			17.98	0.99	17.98	0.99
1.5			20.69	1.18	20.69	1.18
1.6			33.28	1.70	33.28	1.70
1.7			32.35	1.62	32.35	1.62
1.8			43.13	2.34	43.13	2.34
1.9			19.00	1.63	19.00	1.63
2.0			19.90	1.64	19.90	1.64
2.1			16.92	1.57	16.92	1.57

Such a sequence of three cycles is referred to in the following discussion as simply an ionization *cycle*, meaning that it is the smallest cycle of measurements which yields the relative ionization cross section.

For each reduced velocity, the ionization cycle was repeated 25 times, which resulted in 25 values for the relative ionization cross sections. Such a group of ionization cycles together with background measurement cycles is referred to as an ionization *measurement*. The mean cross section and its error estimate were calculated from each ionization measurement at a given reduced velocity. The measurement was repeated again for the next reduced velocity, and such a group of measurements carried over the velocity range is referred to as an ionization *run*. A total of 10–15 ionization runs for each target state was carried out with each of the ion sources. The total data-taking period extended over nine months and occupied approximately 160–170 h of data gathering time, exclusive of tests, setup, rejected runs, etc.

The calculation of the relative ionization cross section from the experimental data was performed as follows for each ionization measurement at reduced velocity $\tilde{v}$. The number of background pulses N_B was subtracted from each of the numbers N_{L+I}, N_L, and N_I in 25 cycles. The SFI areas A_{L+I}, A_L and ion currents I_{L+I}, I_I were also measured in 25 cycles. For each cycle the relative ionization cross section was calculated from

$$\sigma^{\text{ion}} = C_r \left(\frac{N'_{L+I}}{A_{L+I} I_{L+I}} - \frac{N'_L}{A_L I_{L+I}} - \frac{N'_I}{A_{L+I} I_I} \right), \tag{3}$$

where C_r is a coefficient in the run r, N' is a background-subtracted number of pulses, and subscripts denote the corresponding regimes under which the quantities were measured. Finally, the mean ionization cross section and the error of the mean were estimated for each ionization measurement at the reduced velocity $\tilde{v}$.

For each ionization run the coefficient C_r in Eq. (3) was assumed to be constant for all reduced velocities $\tilde{v}$. This constant combined the effects of various parameters of the experimental setup which did not depend on the ion current and population of Rydberg states. The parameters included geometrical characteristics of the experimental setup which did not vary on a day-to-day basis, such as efficiency of collecting electrons into the CEM and cross sectional area of the ion beam, as well as variable settings which could be changed on a day-to-day basis, such as duration of counting window, the CEM efficiency (controlled by the CEM voltages), and the discriminating fraction. These factors also included parameters associated with the detection of the SFI pulse, such as the gain of the EMT, and the gain of the amplifier and sensitivity of the digital oscilloscope.

From run to run, the coefficient C_r changed because of adjustments in the experimental setup parameters just described. The adjustments were necessary to maximize the net signal in each run. After adjustments were made, the parameters were kept constant, and the cross sections in one ionization run for all $\tilde{v}$ were on the same scale, which was defined by the coefficient C_r. The coefficients C_r are *a priori unknown* and were determined on a relative scale by consistency, as determined by a weighted least-squares fitting method that matches the relative velocity dependence of ionization data.

The main source of uncertainty was the Poisson distribution of the CEM counts. The average number of pulses collected during 256 laser shots in a 5-μsec window was a few thousand (between 10^3 and 3×10^3). Therefore, the uncer-

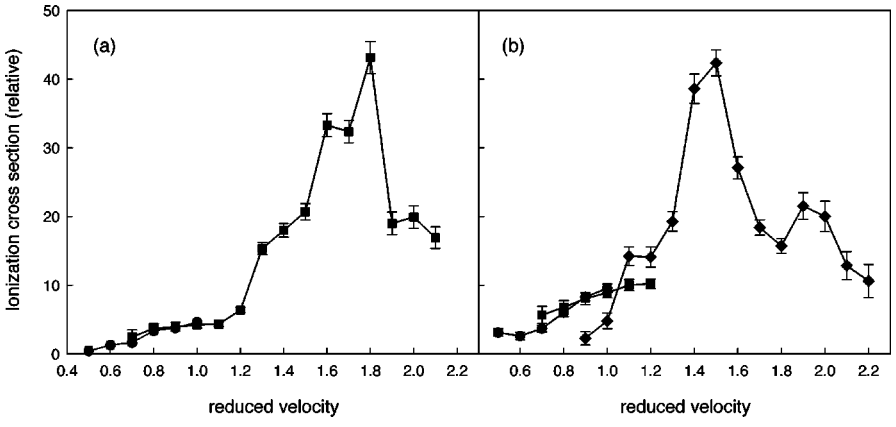

FIG. 3. Relative cross section σ^{ion} vs reduced velocity $\tilde{v}$ for ionization of sodium atom: (a) in the 24*d* state; (b) in the 25*s* state. (a) and (b) Solid circles, K^+ data; solid squares, Na^+ data; (b) only: solid diamonds, Li^+ data. The data points are joined by lines to guide the eye.

TABLE II. Relative ionization cross sections for Na(25*s*) states. SD, standard deviation.

Reduced velocity $\tilde{v}$	σ^{ion} For K^+	SD	σ^{ion} For Na^+	SD	σ^{ion} For Li^+	SD	σ^{ion} For all ions	SD
0.5	37.43	6.01					37.43	6.01
0.6	31.31	6.55					31.31	6.55
0.7	44.18	6.00	68.15	14.98			47.50	5.57
0.8	72.09	6.83	81.15	11.78			74.37	5.90
0.9	99.49	6.73	96.83	10.45	27.52	11.80	85.42	5.10
1.0	114.54	7.48	106.73	9.05	57.59	13.88	103.45	5.33
1.1			120.15	9.92	170.88	16.08	134.14	8.44
1.2			122.49	8.68	169.07	17.60	131.61	7.79
1.3					231.40	17.23	231.40	17.23
1.4					463.04	25.44	463.04	25.44
1.5					508.20	22.82	508.20	22.82
1.6					324.85	19.16	324.85	19.16
1.7					220.66	13.41	220.66	13.41
1.8					188.88	12.74	188.88	12.74
1.9					258.34	23.28	258.34	23.28
2.0					240.09	26.71	240.09	26.71
2.1					154.17	24.64	154.17	24.64
2.2					127.34	29.00	127.34	29.00

tainties associated with the counting statistics were between 30 and 60 pulses on each cycle, corresponding to relative uncertainties between 2% and 3% in the raw signals.

The net signal attributable to impact ionization was between 100 for 1000 total pulses and 600 for 3000 total pulses, or in terms of the signal-to-noise ratio, between 1:10 and 1:5, approximately. Due to propagation of errors in Eq. (3), the variance of the net signal was determined chiefly by the two large values, N_{L+I} and N_L, obtained with the laser ON. The standard deviation of the net signal count was between 50 and 80 and, consequently, the relative uncertainty in ionization cross section was poor, between 10% and 50%.

Three sets of data obtained with different ion sources for ionization from one state had overlapping regions of reduced velocity. Upon direct plotting, they did not match because of the variations in the experimental conditions (represented by C_r) from one ion source to another. (The reason they did not match may be the different ion current-density profiles for the three ion sources. This speculation was justified because the Faraday cup had an aperture of 1.27 cm diameter, and it measured the total current, which could be spread over the full aperture. The total current thus measured left undefined the ion current density actually passing through the cloud of Rydberg atoms, the quantity to which the ionization signal is expected to be proportional.)

Least-squares matching of the velocity dependences was necessary in order to combine these three sets of data, as follows. First, the data obtained with Li^+ ions were chosen as a reference set, and data obtained with Na^+ ions were fitted to Li^+ data in the range of overlapping velocities. Then, the adjusted Na^+ set of data was chosen as a reference set in turn, and the procedure of weighted least-squares fitting was repeated for data obtained with K^+ ions. Finally, after the fitting procedure was performed, all the data for ionization from one state, 25*s* or 24*d*, were combined, and an error estimate of the mean was calculated.

A summary of the results for ionization of Na(24*d*) states in the reduced velocity range $\tilde{v}=0.5$–2.1 is presented in Table I and in Fig. 3(a). A summary of the results for ionization of Na(25*s*) states in the reduced velocity range $\tilde{v}=0.5$–2.2 is presented in Table II and in Fig. 3(b). Three sets of data with various ions and different experimental setups for each of the two states were combined to obtain the summaries.

IV. DISCUSSION

The comparison of the measured relative ionization cross section with scaled theory and CTMC calculations for the Na(24*d*) state is presented in Fig. 4(a) and for the Na(25*s*) state is presented in Fig. 4(b). All cross sections are shown on an absolute logarithmic scale vs reduced velocity $\tilde{v}$. The measured cross sections are shown as dark circles and are scaled to match the absolute CTMC calculations by MacKellar [36] at $\tilde{v}=1.3$.

The solid line is a calculation of total ionization cross section based on a modification of the Rutherford formula that applies to the scattering of two charged particles in the center-of-mass system. The modified Rutherford formula was integrated to obtain the total cross section

$$\sigma_{\text{tot}}=\frac{Z_p^2\pi}{TE_b}\left(\ln\frac{2T}{E_b}\right)^{1/2}, \tag{4}$$

where Z_p is the projectile charge, $T=v^2/2$ is the reduced energy of the projectile, v is the velocity of the projectile, and E_b is the ionization energy of the target ([37], Eq. (3.7), p. 20). Equation (4) was first applied to the ionization of H by protons, and σ_{tot} vs reduced velocity $\tilde{v}$ was found. Then the results were scaled for the Rydberg state with $n^*=n-\delta_\ell$ by multiplying the σ_{tot} by $(n^*)^4$. The reduced energy

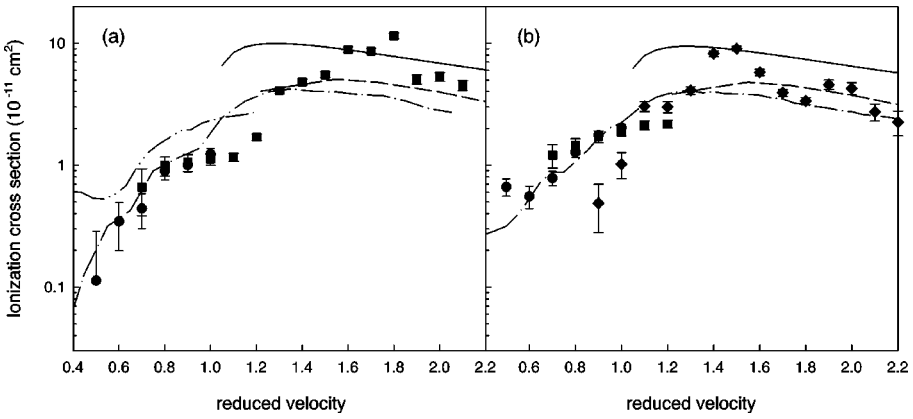

FIG. 4. Comparison of experimental data and theory for ionization of sodium: (a) in the 24*d* state; (b) in the 25*s* state. Experimental data are normalized to the calculation of Ref. [36] at $\tilde{v}=1.3$. (a) and (b) Solid circles, K^+ data; solid squares, Na^+ data; (b) only: solid diamonds, Li^+ data; (a) and (b) solid line, scaled Rutherford formula (Ref. [37]); dashed line, scaled CTMC (Refs. [38,39]); dash-dotted line, absolute CTMC ($m_\ell=0$ for 24*d*) (Ref. [36]); (a) only: dash-dot-dotted line, absolute CTMC, m_ℓ averaged (Ref. [40]).

of the projectile was calculated for the $p+H$ system in the center-of-mass system, $T_{\text{c.m.}}=v^2/4$, where the extra factor 1/2 is due to the reduced mass of the proton-hydrogen system.

The dashed curves are the CTMC calculations of the total ionization cross sections for H^++H collisions by Olson [38,39] scaled by $(n^*)^4$. The energies of the protons in keV were converted to reduced velocities, and σ_{ion} values from [38,39] were multiplied by $(n^*)^4$.

MacKellar [36] and Homan [40] performed CTMC calculations for the ionization cross section of Na Rydberg atoms in 24*d* and 25*s* states by protons in the intermediate reduced velocity region around $\tilde{v}=1$. MacKellar's calculations for the $m_\ell=0$ sublevel of the Na(24*d*) state are shown as a dash-dotted line in Fig. 4(a). [Homan also calculated the ionization cross section from the $m_\ell=0$ sublevel of the Na(24*d*) state of Na in the reduced velocity range $\tilde{v}=0.7-2.0$. Homan's calculations are not plotted since they are almost identical to MacKellar's.] Homan's calculation for the m_ℓ-averaged cross section of the Na(24*d*) state in the reduced velocity range $\tilde{v}=0.4$–1.2 is plotted as a dash-dot-dotted line in Fig. 4(b). The cross sections for ionization from the Na(25*s*) state calculated by MacKellar using the CTMC method are shown as a dash-dotted line in Fig. 4(b).

Analysis of the figures reveals that for both Rydberg states the measured maximum cross section is shifted toward higher reduced velocities relative to theory. In Fig. 4(a) the maximum of the relative ionization cross section is at reduced velocity 1.6–1.7. Interestingly, the scaled CTMC data have a maximum at $\tilde{v}=1.55$, whereas the CTMC calculations performed on Rydberg states (MacKellar) have a maximum at $\tilde{v}=1.35$. It may be due to the fact that only the $m_\ell=0$ sublevel calculation of 24*d* was presented. The calculation of the total ionization cross section by Homan [dash-dot-dotted line in Fig. 4(a)] was carried out only up to $\tilde{v}=1.2$. It remains to be seen how the total ionization cross section would behave around $\tilde{v}=1.4$–1.6.

ACKNOWLEDGMENTS

We would like to thank Carrie Creasey for helpful SIMION calculations. This work was supported in part by NSF Grant Nos. PHY-9413915 and PHY-9704544, and by Research Corporation.

[1] D. R. Bates and G. Griffing, Proc. Phys. Soc. London, Sect. A **66**, 961 (1953).
[2] M. B. Shah and H. B. Gilbody, J. Phys. B **14**, 2361 (1981).
[3] D. S. F. Crothers and J. F. McCann, J. Phys. B **16**, 3229 (1983).
[4] P. D. Fainstein, V. H. Ponce, and R. D. Rivarola, J. Phys. B **23**, 1481 (1990).
[5] P. D. Fainstein, V. H. Ponce, and R. D. Rivarola, J. Phys. B **24**, 3091 (1991).
[6] L. Gulyás, P. D. Fainstein, and A. Salin, J. Phys. B **28**, 245 (1995).
[7] A. Igarashi and T. Shirai, Phys. Rev. A **50**, 4945 (1994).
[8] S. Sahoo, K. Roy, N. Sil, and S. Mukherjee, Phys. Rev. A **59**, 275 (1999).
[9] M. B. Shah, D. S. Elliott, and H. B. Gilbody, J. Phys. B **20**, 2481 (1987).
[10] J. Kuang and C. D. Lin, J. Phys. B **29**, 1207 (1996).
[11] J. Kuang and C. D. Lin, J. Phys. B **29**, 5443 (1996).
[12] T. G. Winter and C. D. Lin, Phys. Rev. A **29**, 3071 (1984).
[13] T. G. Winter, Phys. Rev. A **37**, 4656 (1988).

[14] G. H. Wannier, Phys. Rev. **90**, 817 (1953).
[15] D. R. Bates and A. E. Kingston, *Advances in Atomic and Molecular Physics* (Academic Press, New York, 1970), Vol. 6.
[16] R. Abrines and I. C. Percival, Proc. Phys. Soc. London **88**, 861 (1966).
[17] R. Abrines and I. C. Percival, Proc. Phys. Soc. London **88**, 873 (1966).
[18] R. E. Olson, J. Phys. B **13**, 483 (1980).
[19] R. L. Becker and A. D. MacKellar, J. Phys. B **17**, 3923 (1984).
[20] A. Jain and T. G. Winter, Phys. Rev. A **51**, 2963 (1995).
[21] B. G. O'Hare, R. W. McCullough, and H. B. Gilbody, J. Phys. B **8**, 2968 (1975).
[22] E. J. McGuire, Phys. Rev. A **3**, 267 (1971).
[23] I. P. Zapesochnyi and I. S. Aleksakhin, Zh. Éksp. Teor. Phys. **55**, 76 (1968) [Sov. Phys. JETP **28**, 41 (1969)].
[24] M. B. Shah, D. S. Elliott, P. McCallion, and H. B. Gilbody, J. Phys. B **21**, 2455 (1988).
[25] M. B. Shah, J. Geddes, B. M. McLaughlin, and H. B. Gilbody, J. Phys. B **31**, L757 (1998).
[26] G. C. Bernardi *et al.*, Phys. Rev. A **40**, 6863 (1989).
[27] G. C. Bernardi, P. Focke, S. Suárez, and W. Meckbach, Phys. Rev. A **50**, 5338 (1994).
[28] M. E. Rudd and D. H. Madison, Phys. Rev. A **14**, 128 (1976).
[29] M. E. Rudd, C. A. Sautter, and C. L. Bailey, Phys. Rev. **151**, 20 (1966).
[30] W. S. Tan, Z. Shi, C. H. Ying, and L. Vušković, Phys. Rev. A **54**, R3710 (1996).
[31] K. B. MacAdam *et al.*, Phys. Rev. A **34**, 4661 (1986).
[32] K. B. MacAdam and M. A. Morrison, Phys. Rev. A **43**, 1345 (1993).
[33] Heatwave, 765 Calabasas Rd, Watsonville, CA 95076.
[34] *Channeltron Electron Multiplier Handbook for Mass Spectrometry Applications*, Galileo Electro-Optics Corporation, Galileo Park, P.O. Box 550, Sturbridge, MA 01566.
[35] D. A. Dahl, *SIMION 3D, Version 6.0* (prepared for U.S. Dept. of Energy, Office of Energy Research, Idaho National Engineering Laboratory, Idaho Falls, ID, 1995).
[36] A. MacKellar (private communications).
[37] N. Stolterfoht, R. D. DuBois, and R. D. Rivarola, *Electron Emission in Heavy Ion-Atom Collisions* (Springer-Verlag, New York, 1997).
[38] R. E. Olson, Phys. Rev. A **27**, 1871 (1983).
[39] R. E. Olson, Phys. Rev. A **33**, 4397 (1986).
[40] D. M. Homan (private communication).